International Journal of Thermal Sciences 90 (2015) 38–52

Contents lists available at ScienceDirect

International Journal of Thermal Sciences

journal homepage: www.elsevier.com/locate/ijts

Investigation of the condensation process of moist air around horizontal pipe

A. Fouda [a, b, *], M.G. Wasel [b], A.M. Hamed [b], El-Shafei B. Zeidan [b], H.F. Elattar [c]

[a] Department of Mechanical Engineering, Faculty of Engineering, University of Jeddah, Jeddah, Saudi Arabia
[b] Department of Mechanical Power Engineering, Faculty of Engineering, Mansoura University, Mansoura, Egypt
[c] Department of Mechanical Engineering, Benha Faculty of Engineering, Benha University, Benha, 13511 Qalyubia, Egypt

ARTICLE INFO

Article history:
Received 22 June 2014
Received in revised form
11 November 2014
Accepted 19 November 2014
Available online

Keywords:
Condensation process
Moist air
Horizontal pipe
Heat and mass transfer coefficients

ABSTRACT

The condensation process of water vapor from moist air flowing around horizontal pipe is investigated theoretically and experimentally. This process involved in many engineering applications, such as refrigeration and air conditioning. In the theoretical analysis, the flow is assumed to be laminar, steady and with constant physical properties. The condensation process is described by continuity, momentum, energy and mass in the form of dimensionless ordinary differential equations using similarity variables. The dimensionless governing equations are solved by Runge Kutta fourth order integration technique accompanied with shooting method. The boundary layer thickness of mass, thermal and hydrodynamic, in addition to Nusselt and Sherwood numbers are investigated at different Reynolds numbers, and condensation and position parameters. In the experimental work, the effects of air inlet conditions (i.e. relative humidity, and mass flow rate) are varied and examined on the condensation process. The findings show that the average heat and mass transfer coefficients increase with increasing air mass flow rate and air relative humidity, and decrease with increasing the temperature difference between the air dew point and pipe surface temperature. Comparisons between the present theoretical and experimental work with previous theoretical study are accomplished within accepted error.

1. Introduction

Condensation process from moist air is widely employed in heat exchanger devices such as desalination units, refrigeration units, petroleum refinery and food industries. The heat and mass transfer process associated with condensation over flat plate and around pipe is important for many industrial applications. Condensation process over flat plate and around horizontal pipe was studied by many researchers. The condensation from moist air (including mass transfer) has less attention and seems to need more effort seeking for good understanding of this process. Gaddis and Rose [1,2] studied the condensation of steam on horizontal pipe. Yaghoubi, Kazeminejad [3] studied the effect of inlet relative humidity of moist air over horizontal flat plate. Legay-Desesquelles [4] studied the effect of temperature difference between the inlet temperature of moist air and surface temperature over horizontal flat plate. Condensation of moist air on horizontal pipe is studied by Ref. [5], the study was unsteady state condition for flow under supersaturated frosting. Heat transfer with condensation of water vapor from moist air was investigated by Refs. [6–22]. Cheng and Junming [23] presented a numerical investigation for condensation of humid air along a vertical plate using mathematical model built on the full boundary layer equations and the film-wise condensation assumption. Wilson and Newell [24] performed an experimental investigation to examine the combined buoyancy driven heat and mass transfer in open cavities of different aspect ratios. Sakakura and Yamamoto [25] investigated a numerical study of condensate flows of moist air in a cooled pipe by using the preconditioning method for solving incompressible and compressible Navier–-Stokes equations with additional equations and source terms for condensate flows. Xiaojun et al. [26] illustrated that the indoor moisture distribution, especially for wall condensation, is very important for a healthy and energy-efficient environment. Zhixiang et al. [27] investigated ambient air condensation on a cryogenic horizontal tube using a newly built mathematical model, in which the liquid film and the vapor boundary layer are coupled together

* Corresponding author. Department of Mechanical Engineering, Faculty of Engineering, University of Jeddah, Jeddah, Saudi Arabia. Tel.: +966 530541920 (mobile).
E-mail address: aafoudah@kau.edu.sa (A. Fouda).

http://dx.doi.org/10.1016/j.ijthermalsci.2014.11.022
1290-0729/

Nomenclature

A	surface area, m^2
a	pipe radius, m
d	pipe diameter, m
C_P	specific heat of moist air, kJ/kg °C
L	pipe length, m
h	heat transfer coefficient, kW/m^2 °C
h_m	mass transfer coefficient, m/s
$\dot{m}_a$	mass flow rate of moist air, kg/s
$\dot{m}_c$	rate of condensation, kg/s
Q	total heat transfer, kW
RH	relative humidity of moist air
i	specific enthalpy of moist air, kJ/kg
U_∞	air free stream velocity, m/s
u	velocity component in x-direction, m/s
v	velocity component in y-direction, m/s
T	temperature of air, K
P	air pressure, Pa
K	thermal conductivity, W/m °C
h_{fg}	latent heat of condensation, kJ/kg
w	humidity ratio, kg_w/kg_a
D	mass diffusivity, m^2/s
f	function ($f = u/U_\infty$)
ΔT	temperature difference between dew point and wall temperature, °C
TR	temperature ratio, $TR = \Delta T/(T_{in} - T_w)$

Greek symbols

α	thermal diffusivity, m^2/s
ρ	density, kg/m^3
μ	dynamic viscosity, kg/m s
δ	film thickness, mm
θ	dimensionless temperature
ϕ	dimensionless concentration
υ	kinematic viscosity, m^2/s
Ψ	stream function
ζ	condensation parameter
ξ	position parameter
β	position angle, degree
η	transform axis y
λ	constant; λ is equal zero in the case of no interaction between heat and mass transfer, while λ is equal one when interactions considered

Subscripts

a	air
in	inlet
o	outlet
h	hydrodynamic
t	thermal
m	mass
w	wall
∞	free stream
avg	average value
x	local value

dimensionless quantities

Nu	Nusselt number
Re	Reynolds number
Pr	Prandtl number
Sh	Sherwood number
Sc	Schmidt number

with a major emphasis on the effect of buoyancy. Le et al. [28] derived an analytical solution for the governing equations of steady laminar film condensation from quiescent pure vapors on convex and concave curved vertical walls. Mass transfer of condensable gases and mixtures of laminar films on a flat plate were presented by Ref. [30]. Forced convection condensation in the presence of non-condensables and interface resistance were investigated by Ref. [31]. Heat and mass transfer with condensation of steam-air mixtures were presented by Refs. [32,33]. Forced convection condensation in the presence of a non-condensing gas on a flat plate and horizontal tube was studied by Ref. [34].

According to authors' review, the influence of air mass flow rate, air relative humidity, and temperature difference between air dew point and pipe surface temperature on the heat and mass transfer coefficients of moist air condensation process on the outer surface of horizontal pipe is approximately not fully studied. Consequently, the present work is carried out to investigate the condensation process of moist air on the outer surface of horizontal pipe. In the theoretical study, the influence of Reynolds number and condensation and position parameters on the boundary layer thickness of mass, thermal and hydrodynamic, in addition to Nusselt and Sherwood numbers, are investigated. In other side, the effects of air inlet conditions (i.e. relative humidity and mass flow rate) are examined during condensation process. The experimental results are presented at two different values of temperature difference between air dew point and pipe surface temperature of 5 °C & 10 °C. Finally, numerical and experimental correlations for Nusselt and Sherwood numbers are investigated and presented in terms of all studied parameters within accepted error.

2. Theoretical study

The system physical model which is considered in this analysis is illustrated in Fig. 1. In the theoretical analyses of this work, the flow is assumed to be laminar, steady and with constant physical properties, moreover the thicknesses of water vapor layer is small compared with pipe radius. The condensation process is described by continuity, momentum, energy and mass partial differential equations that expressed in Cartesian coordinates system. According to the nature of the studied problem and to proper transformation of the dependent and independent problem variables, the governing equations are transformed to a set of ordinary differential equations (ODE). Therefore, the well-known numerical method, Rung Kutta is applied to solve the set of ODE. In consequence, the boundary layer thickness of mass, thermal and hydrodynamic, in addition to Nusselt and Sherwood numbers at different Reynolds numbers are investigated, Condensation and position parameters are well defined. The physical problem can be described as a humid air flow with inlet velocity (U) and uniform temperature (T) passes around constant surface temperature horizontal pipe. The physical description of the problem and coordinate system is shown in Fig. 1a, and the model in orthogonal curvilinear coordinates is depicted in Fig. 1b.

2.1. Governing equations

According to the foregoing assumptions, the continuity, momentum, energy and mass equations in Cartesian coordinates can be written as:

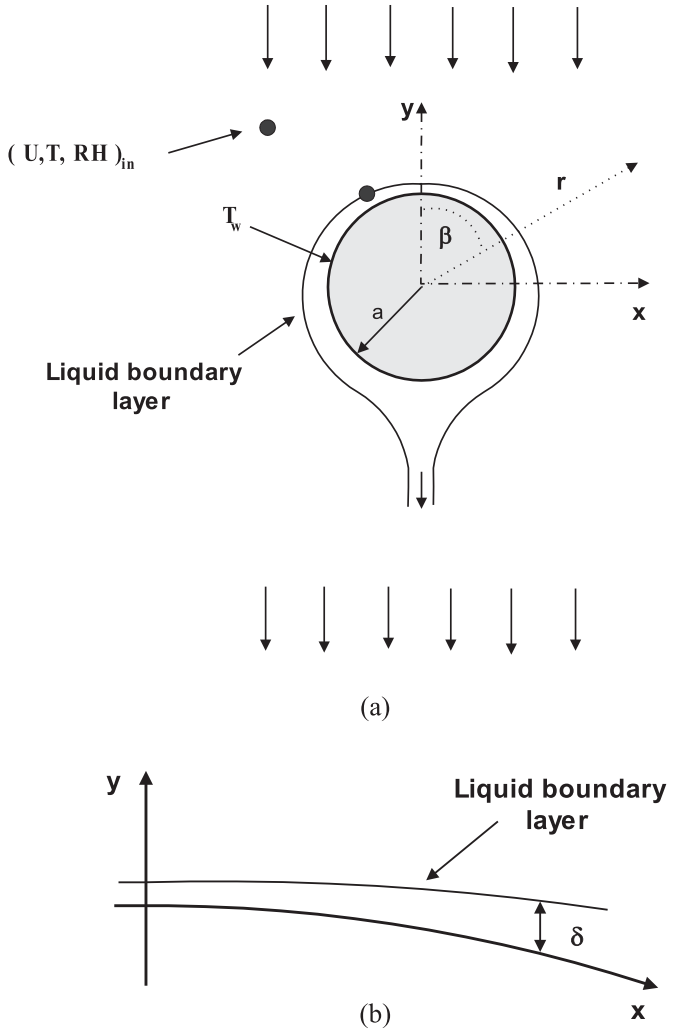

Fig. 1. (a) Physical description of the problem and coordinate system, (b) Model in orthogonal curvilinear coordinates.

$$\frac{\partial u}{\partial x}+\frac{\partial v}{\partial y}=0.0 \tag{1}$$

$$u\frac{\partial u}{\partial x}+v\frac{\partial u}{\partial y}=\upsilon\frac{\partial^2 u}{\partial y^2}+g\sin(\beta) \tag{2}$$

$$u\frac{\partial T}{\partial x}+v\frac{\partial T}{\partial y}=\alpha\frac{\partial^2 T}{\partial y^2}+\lambda D\frac{h_{fg}}{\rho C_p}\frac{\partial^2 \rho}{\partial y^2} \tag{3}$$

$$u\frac{\partial \rho}{\partial x}+v\frac{\partial \rho}{\partial y}=D\frac{\partial^2 \rho}{\partial y^2} \tag{4}$$

In Equation (3), λ is constant and equals zero in the case of no interaction between heat and mass transfer, while λ equals one when interaction is considered.

Equations from (1)–(4) must satisfy the following boundary conditions.

$$\begin{aligned} &At \quad y=0.0\\ &u=v=0.0,\quad T=T_w,\quad \rho=\rho_w \end{aligned} \tag{5}$$

$$\begin{aligned} &At \quad y=\infty\\ &u=U_{\infty,t},\quad T=T_\infty,\quad \rho=\rho_\infty \end{aligned} \tag{6}$$

where, $U_{\infty,t}=2U_\infty\sin(\beta)$.

The velocity, temperature, and density distributions throughout the flow field can be obtained by solving equations from (1)–(4) with boundary conditions ((5) and (6)). Nusselt and Sherwood numbers can be defined as.

$$Nu_x=\frac{hx}{k} \tag{7}$$

$$Sh_x=\frac{h_m x}{D} \tag{8}$$

where $x=a\sin(\beta)$.

2.2. Dimensionless form of the governing equation

Seeking for simplified form of flow governing equations from (1)–(4), the dimensionless forms of dependent and independent variables of the problem are introduced as follows:

$$\eta=\frac{y}{\sqrt{x}}\sqrt{\frac{u_{\infty,t}}{\upsilon}} \tag{9}$$

$$\Psi=\sqrt{u_{\infty,t}\upsilon x}f(\eta) \tag{10}$$

$$u=\frac{\partial \Psi}{\partial y} \tag{11}$$

$$v=-\frac{\partial \Psi}{\partial x} \tag{12}$$

$$\theta=\frac{T-T_w}{T_\infty-T_w} \tag{13}$$

$$\phi=\frac{\rho-\rho_w}{\rho_\infty-\rho_w} \tag{14}$$

where, η, f, θ, and ϕ are similarity variable, stream function ratio, temperature ratio and concentration ratio, respectively. Substituting equations from (9)–(14) in equations from (1)–(4), the dimensionless ordinary differential equations of flow describing equations can be obtained and written as follows:

$$f^{\backslash\backslash\backslash}+0.5ff^{\backslash\backslash}+\xi=0.0 \tag{15}$$

$$\theta^{\backslash\backslash}+0.5\mathrm{Pr}\theta^{\backslash}+\lambda\zeta=0.0 \tag{16}$$

$$\phi^{\backslash\backslash}+0.5Scf\phi^{\backslash}=0.0 \tag{17}$$

where,

$$Pr=\frac{\mu_a c_{pa}}{K_a}\quad \xi=\frac{xg\sin(\beta)}{u_{\infty,t}^2}\quad \text{and}\quad \zeta=\frac{h_{fg}(\rho_\infty-\rho_w)}{\rho Cp(T_\infty-T_w)}\frac{\mathrm{Pr}}{Sc}\phi^{\backslash\backslash}$$

The boundary conditions of the flow described in Equations (5) and (6) can be expressed as:

$$\begin{aligned} &At\ \eta=0.0\\ &f=f^{\backslash}=0.0,\quad \theta=\phi=0.0 \end{aligned} \tag{18}$$

$$At\ \eta = \infty \quad f^{\backslash} = 1.0,\ f^{\backslash\backslash} = 0.0,\ \theta = \phi = 1.0 \tag{19}$$

where, $f^{\backslash} = u/U_{\infty,t}$

The local Nusselt and Sherwood numbers in terms of dimensionless variables can be defined as:

$$Nu_x = \left.\frac{\partial\theta}{\partial\eta}\right|_{\eta=0.0}\sqrt{Re_x} \tag{20}$$

$$Sh_x = \left.\frac{\partial\phi}{\partial\eta}\right|_{\eta=0.0}\sqrt{Re_x} \tag{21}$$

The average values of Nusselt and Sherwood numbers can be evaluated by integration of the local values over the pipe surface, hence:

$$Nu_{avg} = \frac{1}{L}\int_0^L Nu_x dx \tag{22}$$

$$Sh_{avg} = \frac{1}{L}\int_0^L Sh_x dx \tag{23}$$

2.3. Numerical procedure

Equations from (15) and (16) are not coupled, i.e. each one can be solved separately. Since these equations are ODE, (boundary value problems type). The ODE can be solved using Runge Kutta fourth order integration technique accompanied with shooting method.

The momentum Equation (15) and its associated boundary conditions ((18) and (19)) can be replaced by the following three first-order ordinary differential equations:

$$f^{\backslash} = V \tag{24}$$

$$V^{\backslash} = Z \tag{25}$$

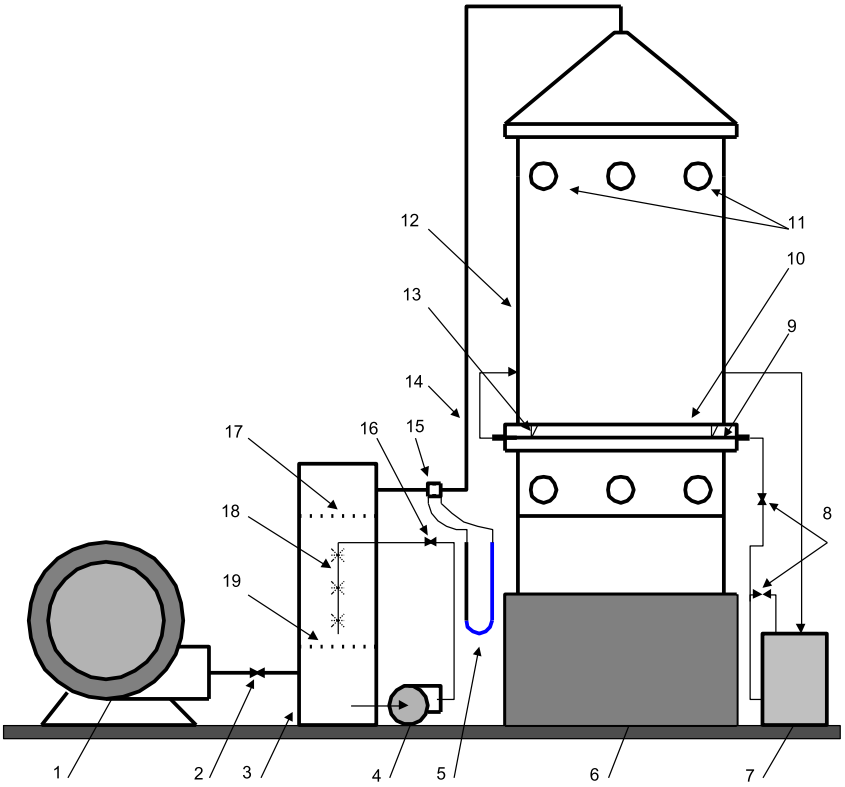

1- Air blower	5- U tube manometer	9- Horizontal pipe	13- Thermocouple
2- Gate valve	6- Base	10- Test section	14- PVC pipes
3- Humidifier	7- Refrigeration unit	11- Measurements holes	15- Orifice meter
4- Pump	8, 16- Control valves	12- Air duct	17, 19- Screen
			18- Water injector

Fig. 2. Experimental setup layout.

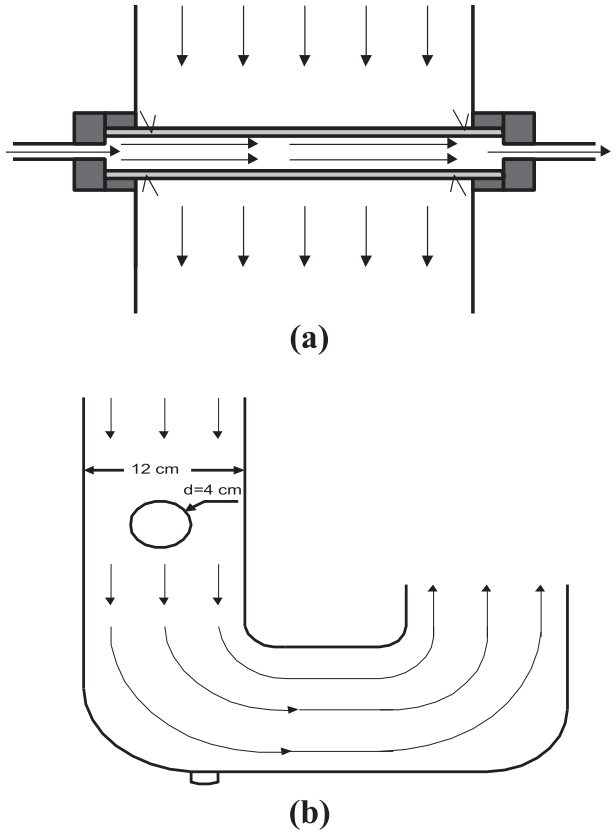

Fig. 3. Test section: (a) front view, (b) side view.

$$Z' = -0.5fZ - \xi \tag{26}$$

These equations must satisfy the following boundary conditions:

$$f(0) = 0.0,\ V(0) = 0.0,\ V(\infty) = 1.0,\ Z(\infty) = 0.0 \tag{27}$$

It is clear from Equations (24)–(27) that the value of the variable $Z(0)$ must be assumed as a first guess. Runge Kutta fourth order method for solving Equations (24)–(26) at different values of position parameter, ξ is used. Similarly, the procedure is applied to solve Equations (16) and (17) for energy and mass, respectively.

3. Experimental study

3.1. Experimental setup

The experimental setup is designed and established to study the parameters affecting the condensation process of moist air on the horizontal pipe as shown in Fig. 2. It consists mainly of Air blower (1), humidifier (3), refrigeration unit (7) and test section (10). To control the mass flow rate of inlet air, throttle valve (2) is fitted between the humidifier inlet and the exit of air blower. Water circulating pump (4) is used to supply water to water injector (18)

Table 2
Instrumentations technical specifications.

Instrumentation	Measured value	Resolution	Span	Accuracy
Anemometer	Air flow velocity	0.01 m/sec	0.7: 25 m/sec	±2%
	Temperature	0.1 °C	−10: 50 °C	±0.6 °C
K-type thermocouple	Temperature	1 °C	−100 to 0 °C	±5 °C
			0–1370 °C	±(0.1% + 2 °C)
Hygrometer	Humidity	0.1%	0–95%	±3% + 1 RH% for >70% RH ± 3% for <70% RH
	Temperature		0–100 °C	±1.8%

Table 3
Values of the uncertainty in calculated parameters.

Calculated Parameters	Uncertainties
Air humidity ratio, w_a	$w_{w_a}/w_a = \pm 0.041$
Air mass flow rate, $\dot{m}_a$	$w_{\dot{m}_a}/\dot{m}_a = \pm 0.073$
Condensation and heat transfer surface area, A	$w_A/A = \pm 0.025$
Rate of condensation, m_c	$w_c/m_c = \pm 0.09638$
Total heat transfer, Q	$w_Q/Q = \pm 0.0524$
Average heat transfer coefficient, h_{avg}	$w_{h_{avg}}/h_{avg} = \pm 0.0752$
Average mass transfer coefficient, $h_{m,avg}$	$w_{h_{m,avg}}/h_{m,avg} = \pm 0.0423$
Average Nusselt number, Nu_{avg}	$w_{Nu_{avg}}/Nu_{avg} = \pm 0.121$
Average Sherwood number, Sh_{avg}	$w_{Sh_{avg}}/Sh_{avg} = \pm 0.113$

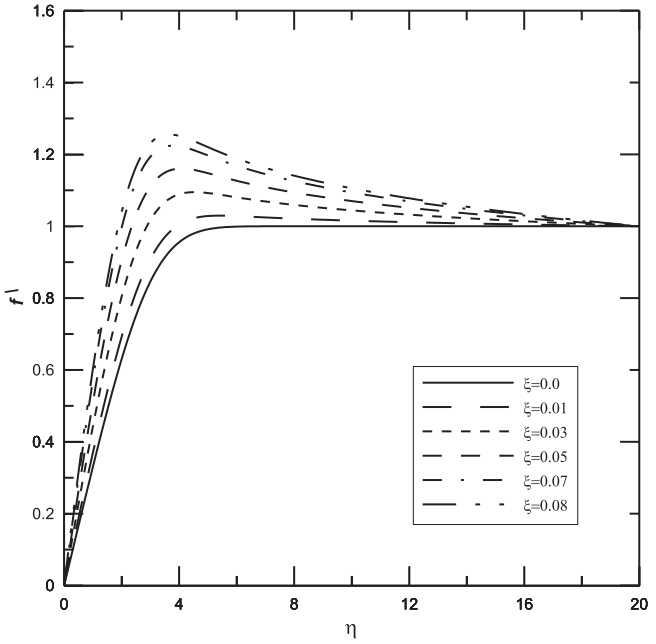

Fig. 4. Boundary layer velocity distribution.

Table 1
Main experimental measured and calculated parameters.

Measured parameters	$T_{w,in}$ (°C)	$T_{w,out}$ (°C)	T_{wal} (°C)	$RH_{a,out}$ (%)	$T_{a,out}$ (°C)	$RH_{a,in}$ (%)	$T_{a,in}$ (°C)	ΔT (°C)	m_a (kg/s)
Calculated parameters	$W_{a,in}$ (kg_{wv}/kg_{da})	$W_{a,out}$ (kg_{wv}/kg_{da})	$h_{a,out}$ (kJ/kg_{da})	$h_{a,in}$ (kJ/kg_{da})	$h_{m,avg}$ (m/s^2)	h_{avg} (W/m^2 K)	m_c (kg/s)	Sh_{avg}	Nu_{avg}

for humidifying air. The humidifier contains barriers (eliminators) to prevent water droplets from passing through the test section to avoid the undesirable effects on the condensation process. An orifice meter (15) is used to measure the flow rate of air stream. The air duct (12) has a rectangular cross section with dimensions of 12 cm × 100 cm. As shown in Fig. 3 the test section consists of a horizontal copper pipe (9) of 4 cm diameter and 100 cm length, the pipe is located in the center of the duct (12) crossing the air flow. Condensation surface temperature is measured using six thermocouples uniformly distributed on the pipe surface. The moist air enters from the top of the supply air duct and exits to atmosphere via a return bend duct as seen in Fig. 3b.

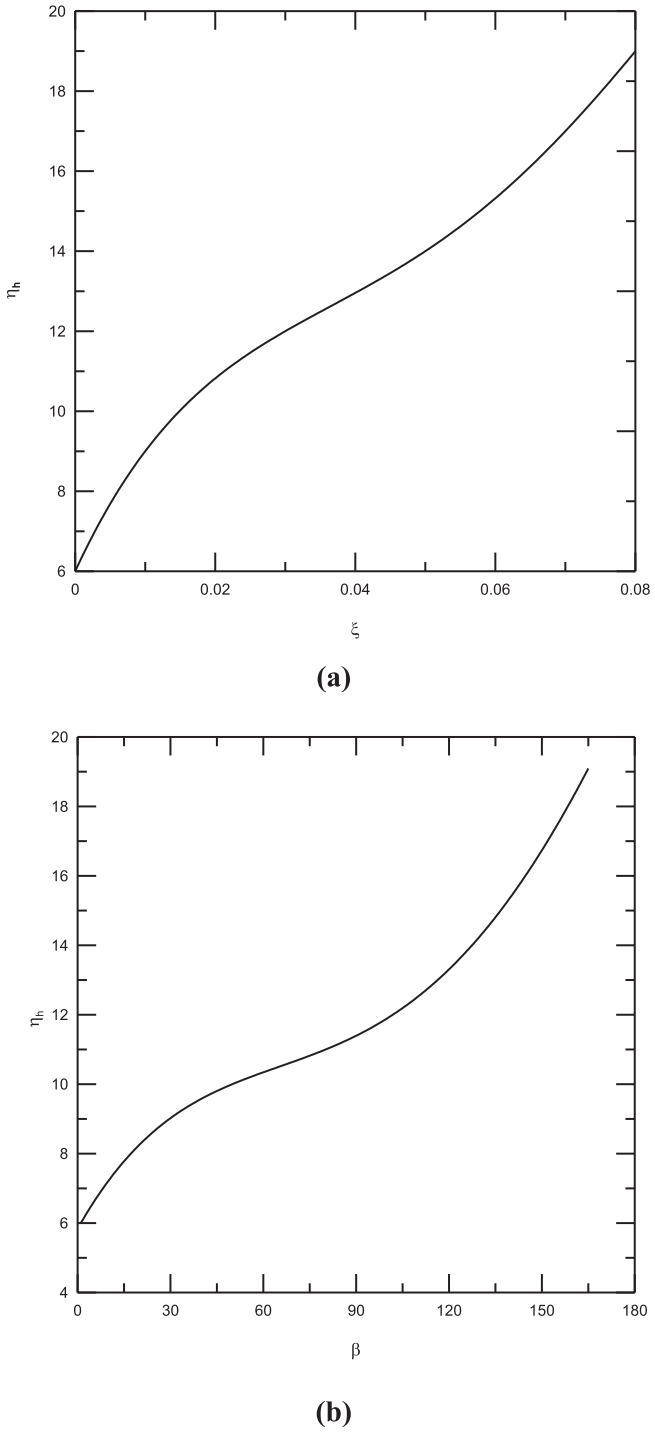

Fig. 5. Hydrodynamic boundary layer thickness versus; (a) position parameter, (b) position angle.

3.2. Experimental measurements

The relative humidity, dry bulb temperature, air mass flow rate and temperature difference between the air dew point and pipe surface are measured during the experiments. In addition to, orifice meter, digital thermometer, thermocouples (k-type), hygrometer, and anemometer are used. Orifice meter (15) is used to measure the air flow rate. The digital hygrometer has resolution of 0.1% for relative humidity and 0.1 °C for temperature. The air temperature and relative humidity are obtained from the average of twelve measuring points located at upstream and downstream of the test section distributed uniformly across the duct section. Condensation surface temperature is measured using six thermocouples uniformly distributed on the pipe surface. The main experimental measured and calculated parameters are presented in Table 1. The detailed technical specifications of instruments used in the experimental setup are presented in Table 2.

3.3. Analyses of experimental data

From measuring the air temperatures, relative humidities at upstream and downstream of the test section and air mass flow rate, the average heat and mass transfer coefficients, condensation rate, Nusselt and Sherwood numbers can be calculated as follows:

$$\dot{m}_c = \dot{m}_a(w_{\text{in}} - w_{\text{out}}) \tag{28}$$

$$h_{m,\text{avg}} = \frac{\dot{m}_c}{A(\rho_{\infty,\text{av}} - \rho_w)} \tag{29}$$

$$h_{\text{avg}} = \frac{\dot{m}_a(i_{\text{in}} - i_{\text{out}})}{A(T_{\infty,\text{av}} - T_w)} \tag{30}$$

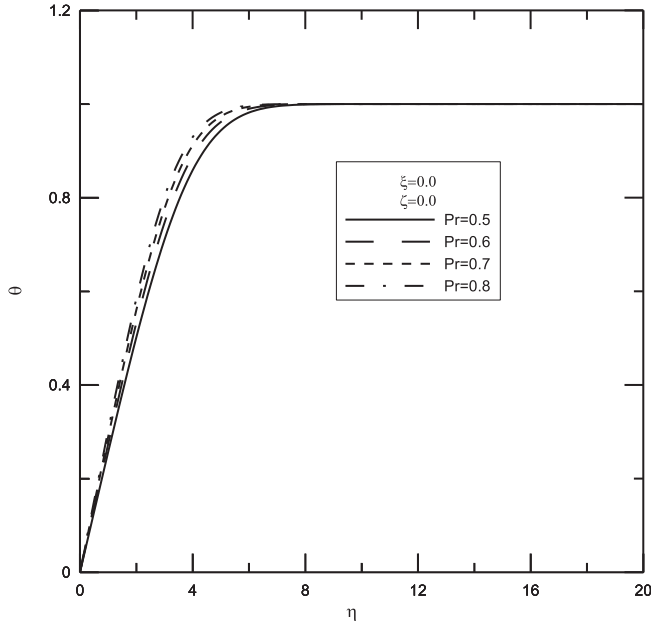

Fig. 6. Effect of Prandtl number on the dimensionless temperature distribution.

$$Re_d = \frac{u_\infty d}{\upsilon} \tag{31}$$

$$Nu_{avg} = \frac{hd}{k} \tag{32}$$

$$Sh_{avg} = \frac{h_m d}{D} \tag{33}$$

The method of estimating uncertainty of experimental results is used for calculating the error in experimental instruments as presented by Refs. [21,22]. This method is based on a careful specification of the uncertainties in the various primary experimental measurements.

Equations 28–33 can be put on the form $R = f(x_1, x_2, x_3,..,x_n)$ where R is the calculated variable and $(x_1, x_2, x_3,..,x_n)$ are the measured parameters. The errors in the measurements of these parameters are depicted in Table 2. The uncertainty in R due to the

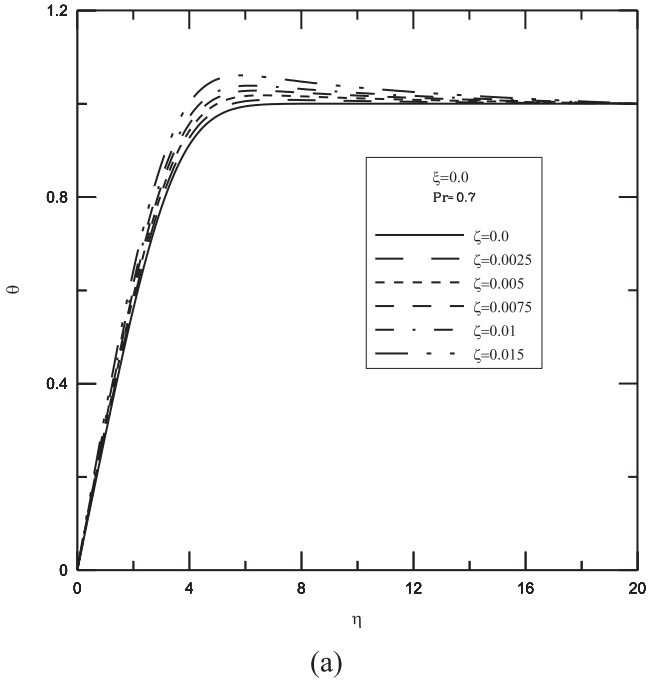

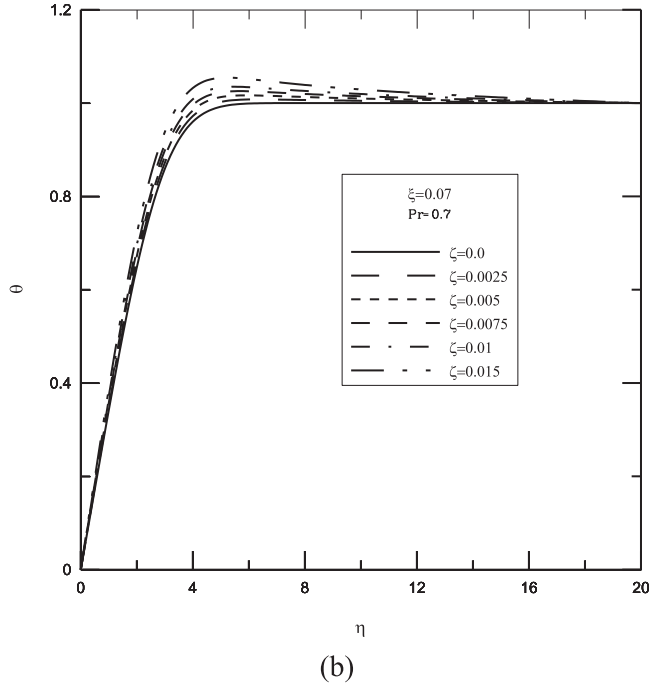

Fig. 7. Effect of condensation parameter on the dimensionless temperature distribution at; (a) $\xi = 0$, (b) $\xi = 0.07$.

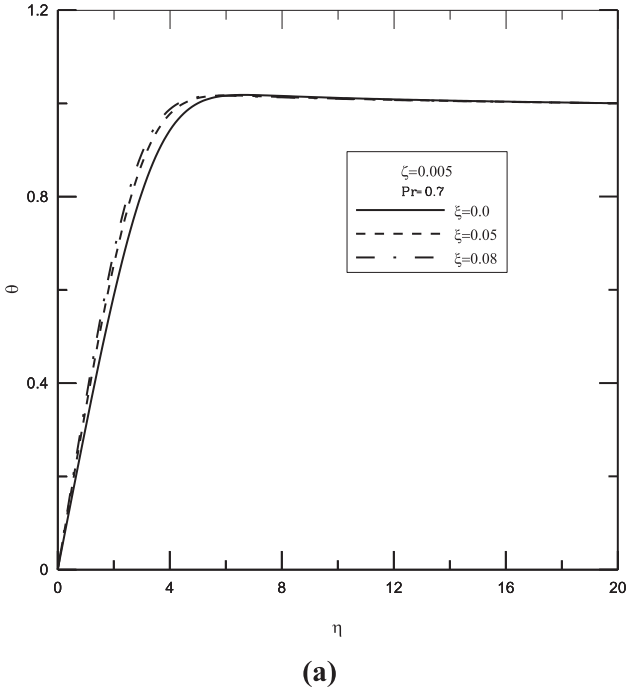

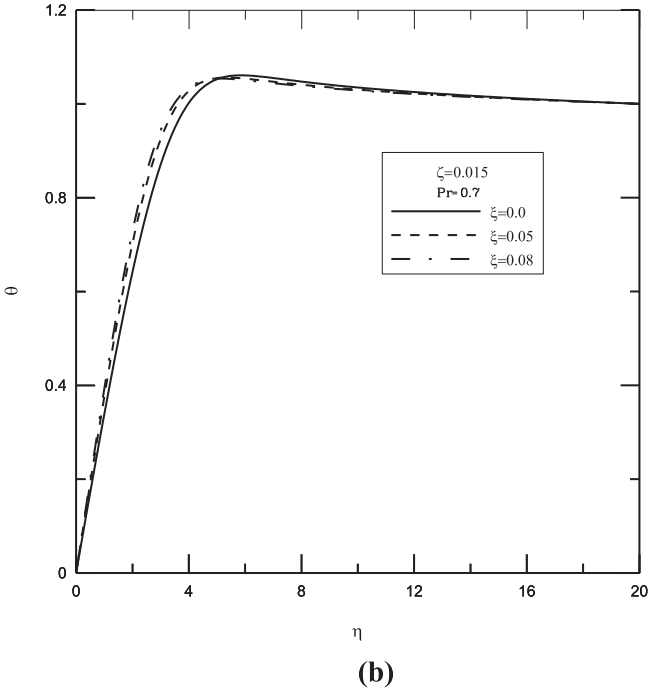

Fig. 8. Effect of position parameter on the dimensionless temperature distribution at; (a) $\zeta = 0.005$, (b) $\zeta = 0.015$.

uncertainties of these parameters can be calculated from Eq. (34) that was given by Holman and Gajda [29].

$$w_R = \left[\left(\frac{\partial R}{\partial x_1}w_1\right)^2 + \left(\frac{\partial R}{\partial x_2}w_2\right)^2 + \ldots\ldots + \left(\frac{\partial R}{\partial x_n}w_n\right)^2\right]^{0.5} \quad (34)$$

where $\partial R/\partial x_i$ is calculated by numerical differentiation using the developed computer program. The values of the uncertainty in calculated parameters are presented in Table 3.

4. Results and discussions

4.1. Theoretical results & discussions

The effects of Reynolds number, Prandtl and Schmidt numbers, and position and condensation parameters on boundary layer thickness of mass, thermal and hydrodynamic, in addition to Nusselt and Sherwood numbers are examined and presented in the following sections.

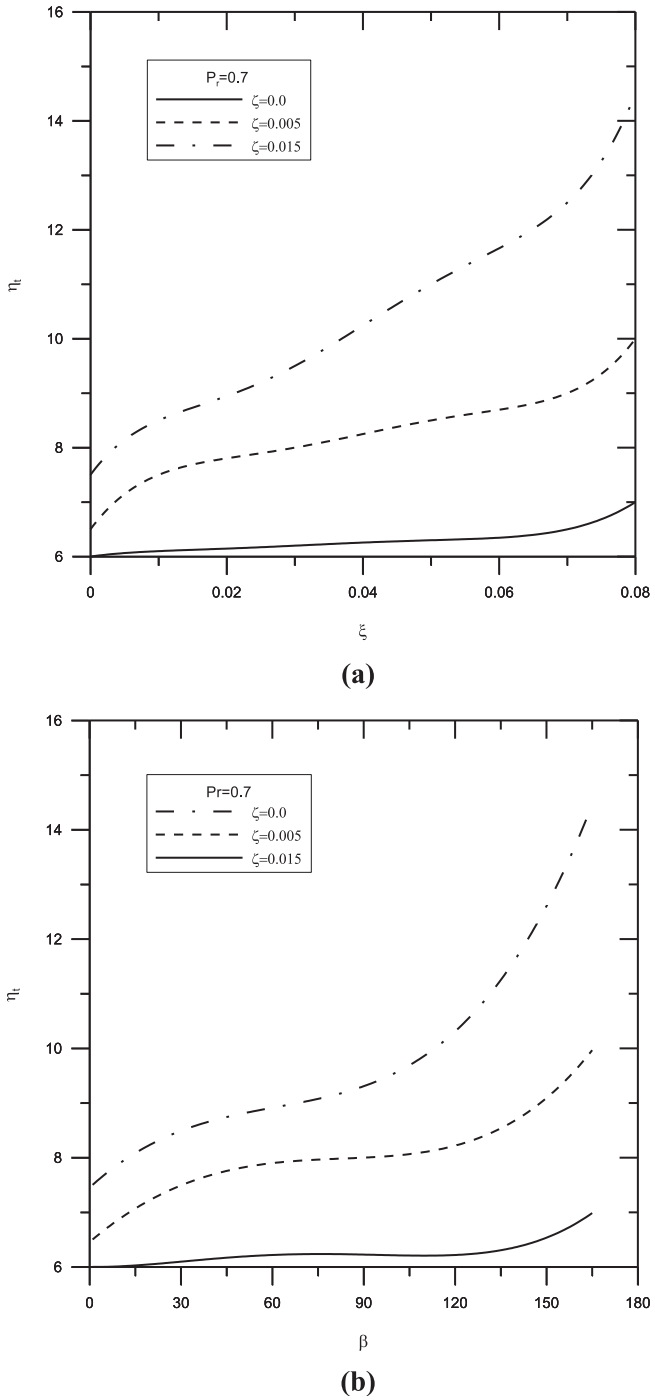

Fig. 9. Thermal boundary layer thickness versus; (a) position parameter, (b) position angle.

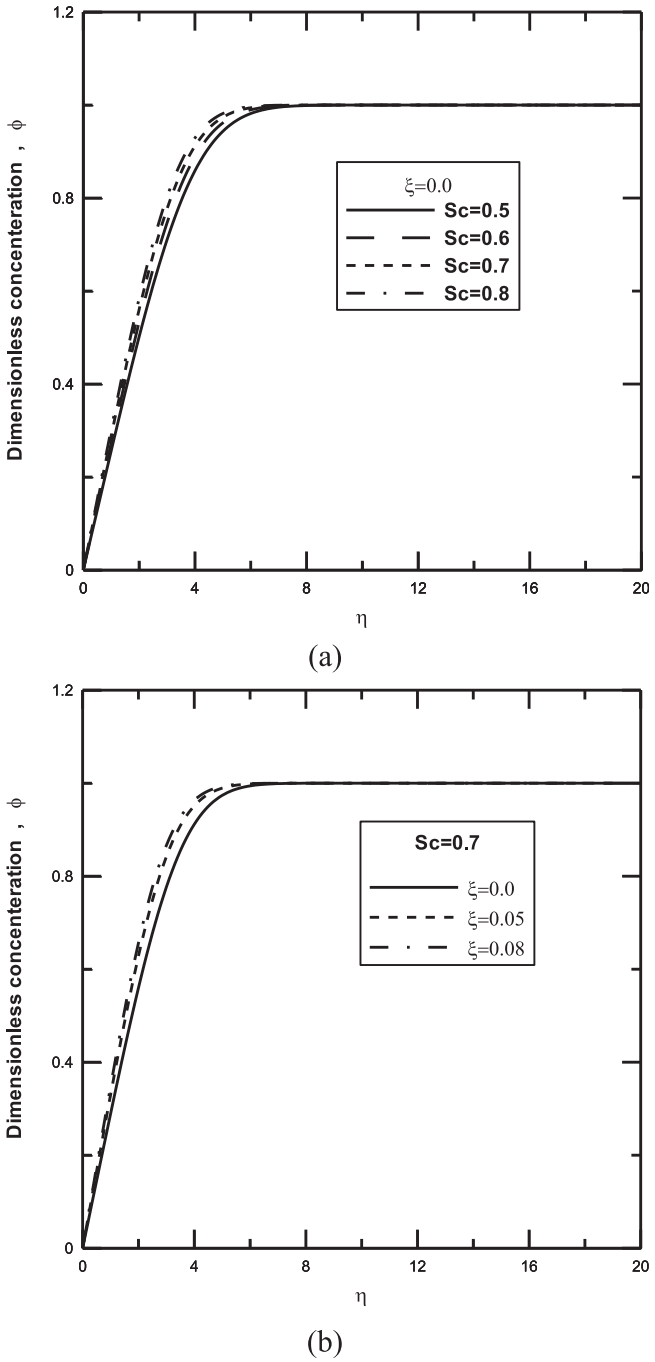

Fig. 10. Dimensionless concentration distribution with different (a) Schmidt number, (b) position parameter.

4.1.1. Boundary layer velocity distribution and its hydrodynamic thickness

To find the boundary layer velocity distribution in hydrodynamic thickness, the velocity ratio, f' is plotted versus the independent variable, η at different values of position parameter, ξ as shown in Fig. 4. As shown in the figure at $\xi = 0.0$, which represents the case of horizontal flat plate, as seen, the f' increases rapidly with increasing η and then reaches approximately to constant value. For $\xi < 0$, the trend of relation between f' and η is the same as $\xi = 0.0$ and it increases with increasing ξ and consequently the hydrodynamic boundary layer thickness, η_h increases which obtained when the velocity ratio f' takes its asymptotic value. The relation of η_h versus ξ is presented in Fig. 5a, where η_h can be obtained from Fig. 4 at asymptotic value of f'. The separation point depends on Reynolds number, where the separation occurs at higher position angle with increasing Reynolds number. In order to obtain the separation point, hydrodynamic boundary layer thickness, η_h is plotted versus position angle β as shown in Fig. 5b, where η_h can be obtained from Fig. 4 at asymptotic value of f'. Where, the separation point approximately equals 170° which determined from the figure.

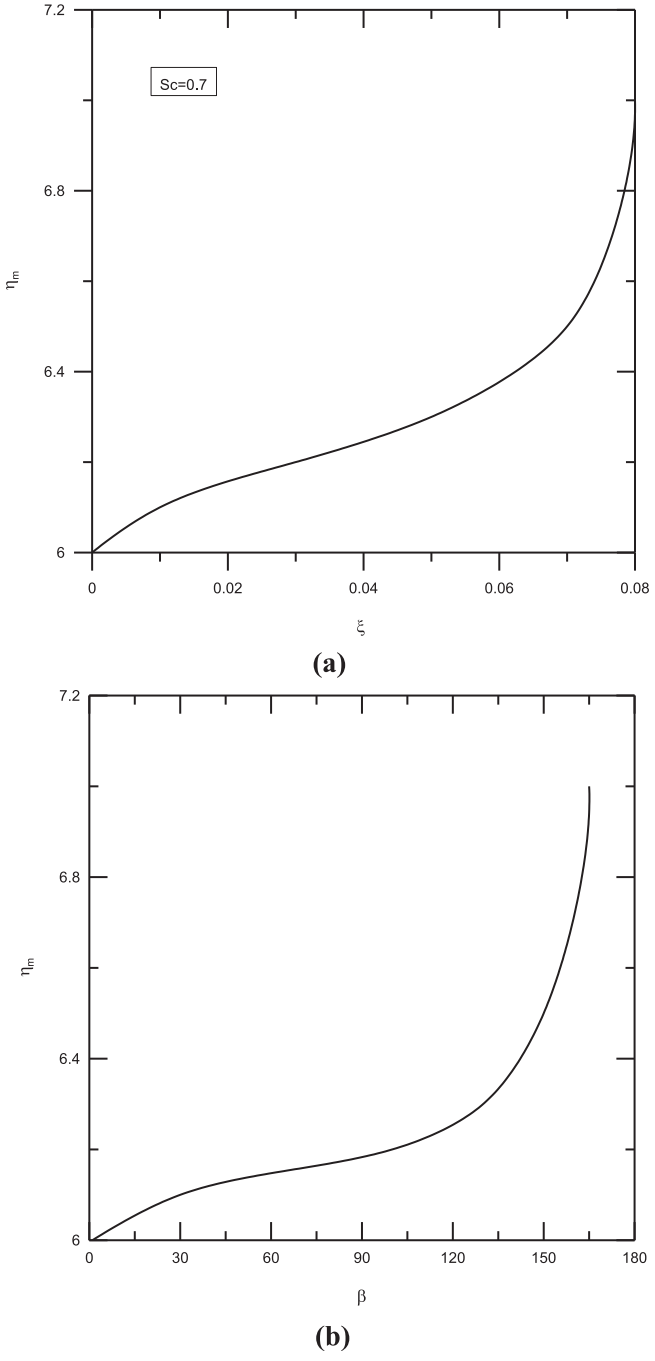

Fig. 11. Mass boundary layer thickness versus; (a) position parameter, (b) position angle.

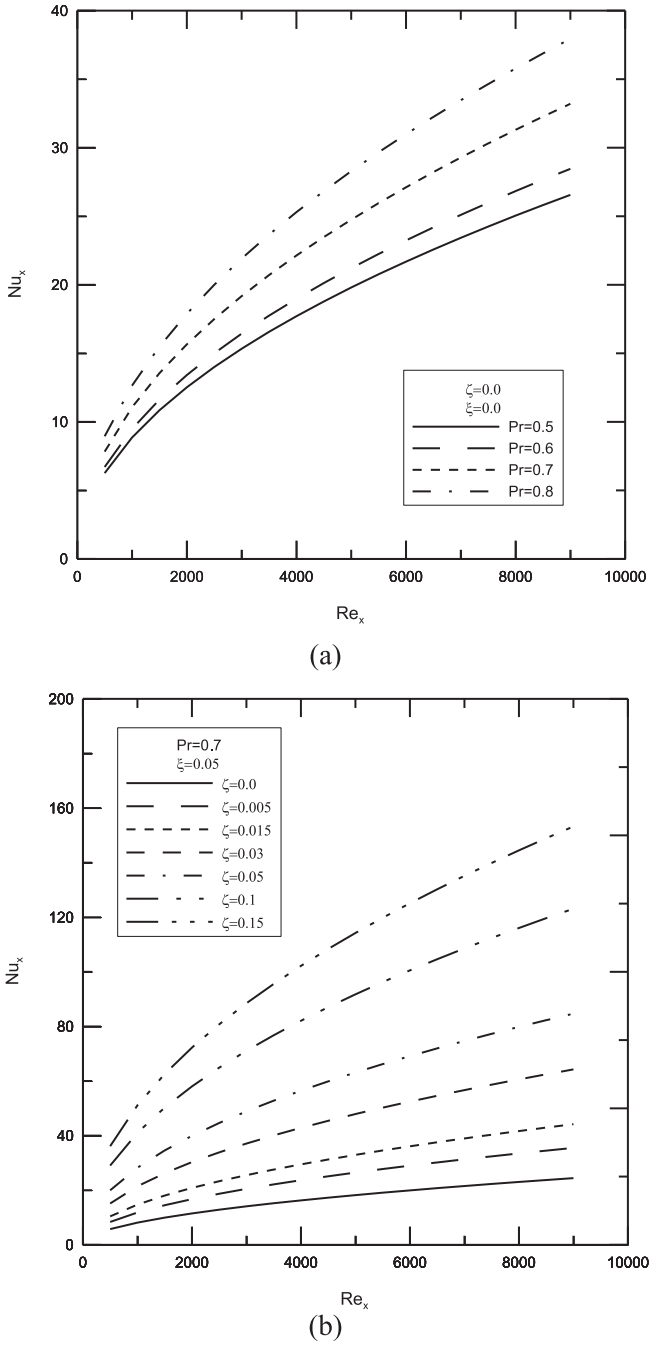

Fig. 12. Nusselt number versus Reynolds number at different: (a) *Pr* number, (b) condensation parameter.

4.1.2. Boundary layer temperature distribution and its thermal thickness

To obtain thermal boundary layer thickness, the dimensionless temperature θ is plotted versus η at different values of Prandtl number. As shown in Fig. 6 at $\xi = \zeta = 0$, for any values of Prandtl number and at $\eta < 7.0$, θ increases remarkably with increasing η and after that it reaches approximately to constant value. Furthermore, at $\eta < 7.0$, θ increases with increasing Pr for any η, otherwise, Pr has approximately no effect on θ. The effects of condensation parameter, ζ on θ at $Pr = 0.7$ and different two values of $\xi = 0$ & 0.07 are shown in Fig. 7a and b, respectively. As shown in the figures, θ increases with increasing ζ, hence the thermal boundary layer thickness, η_t increases. Moreover, the influence of ξ on θ can be neglect and further proofing is illustrated in Fig. 8a and b. The relations of η_t versus ξ and β at different values of ζ as a studied parameter are presented in Fig. 9a and b, respectively, where η_t can be find from Fig. 7 at asymptotic value of θ.

4.1.3. Boundary layer concentration distribution and its mass thickness

The mass boundary layer thickness, η_m can be obtained from plotting the dimensionless concentration, ϕ against η at different values of Schmidt number as a studied parameter. As shown in

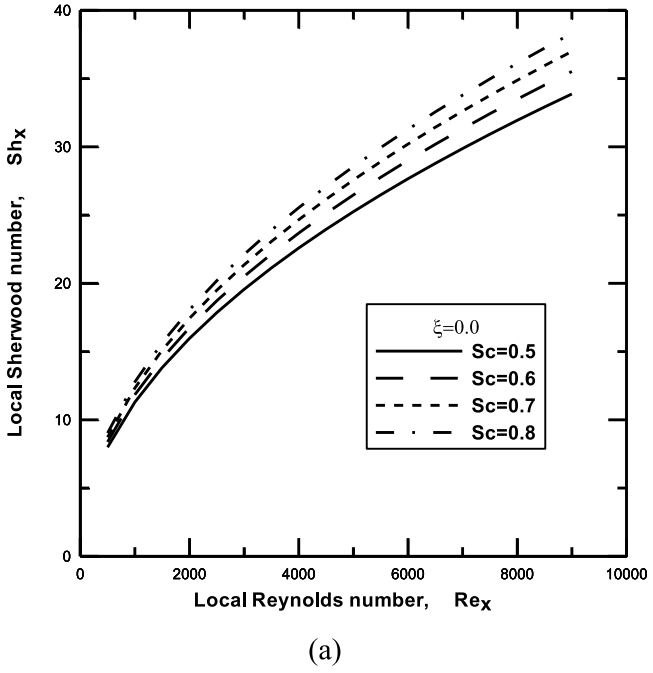

Fig. 13. Sherwood Number versus Reynolds number at different: (a) *Sc* number, (b) position parameter.

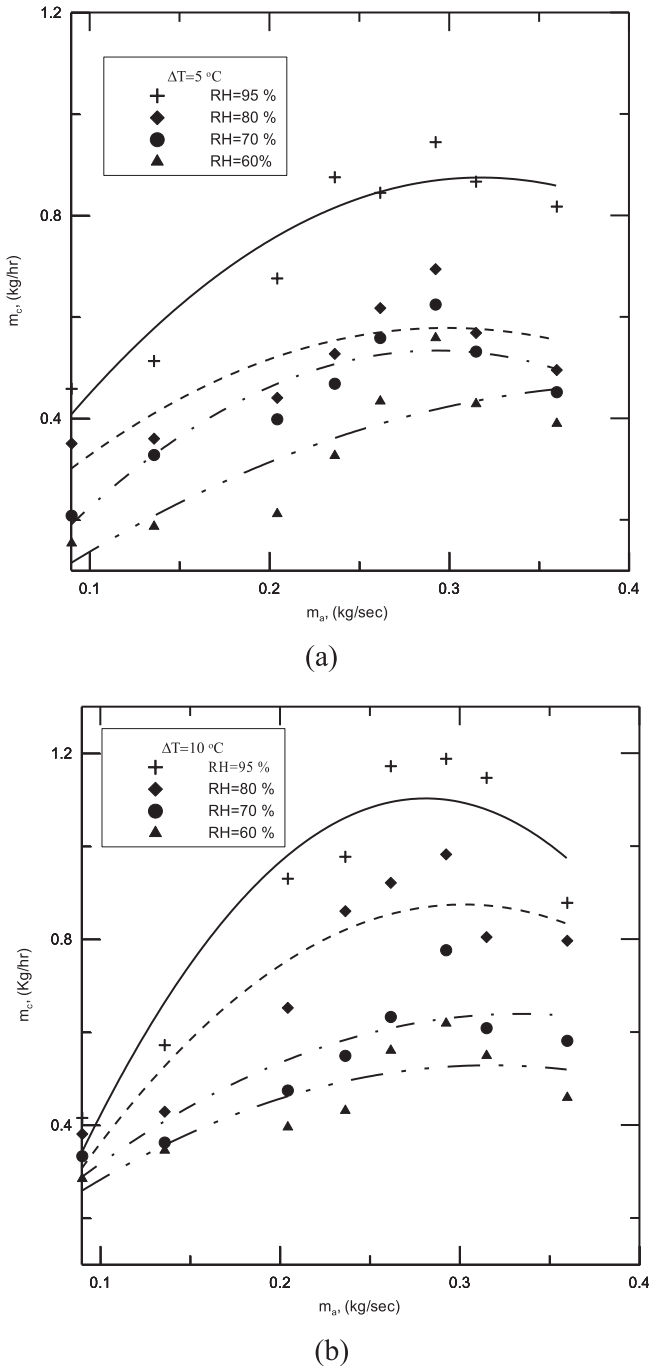

Fig. 14. Rate of Condensation for different values of air relative humidity at: (a) $\Delta T = 5$ °C, (b) $\Delta T = 10$ °C.

Fig. 10a at $\xi = 0$, ϕ increases significantly with increasing η and this trend appears up to $\eta = 7.0$, then, ϕ reaches to an asymptotic value. Moreover, the Schmidt number, Sc has a smaller effect on ϕ for $\eta < 7.0$ and negligible effect for $\eta > 7.0$. Similarly, the effect of position parameter, ξ on ϕ is illustrated in Fig. 10b. The relation of η_m versus ξ and position angle, β are presented in Fig. 11a and b, respectively, where η_m can be find from Fig. 10b at asymptotic value of ϕ.

4.1.4. Local Nusselt and Sherwood Numbers

The relation between the local Nusselt number and Reynolds number at different Prandtl numbers and condensation parameters is shown in Fig. 12a and b, respectively. It can be noted from the figures that at certain Reynolds Number, Re_x the local Nusselt number, Nu_x increases remarkably with increasing both of Prandtl Numbers, Pr and condensation parameter, ζ which results in an increase in condensation rate and consequently the heat generated due to latent heat of condensation increases. Furthermore, the effects of P_r & ζ on Nu_x become significant at higher Re_x, in addition to the influence of ζ on Nu_x is effecter than P_r. In the same way, Schmidt number and position parameter have a considerable increasing effects on Sherwood number and consequently the condensation rate increases with increasing Sc as can be seen in Fig. 13a and b.

4.2. Experimental results & discussions

The effects of air inlet conditions (i.e. relative humidity and air mass flow rate) are varied and examined on the condensation rate, heat and mass transfer coefficients, and the average Nusselt and Sherwood numbers are discussed and presented in the following sections. The results are presented at two different values of temperature difference between air dew point and pipe surface temperature, ΔT of 5 °C & 10 °C.

4.2.1. Rate of condensation

The rate of condensation versus the air mass flow rate at different air inlet relative humidity ranges from 60% to 95% as a

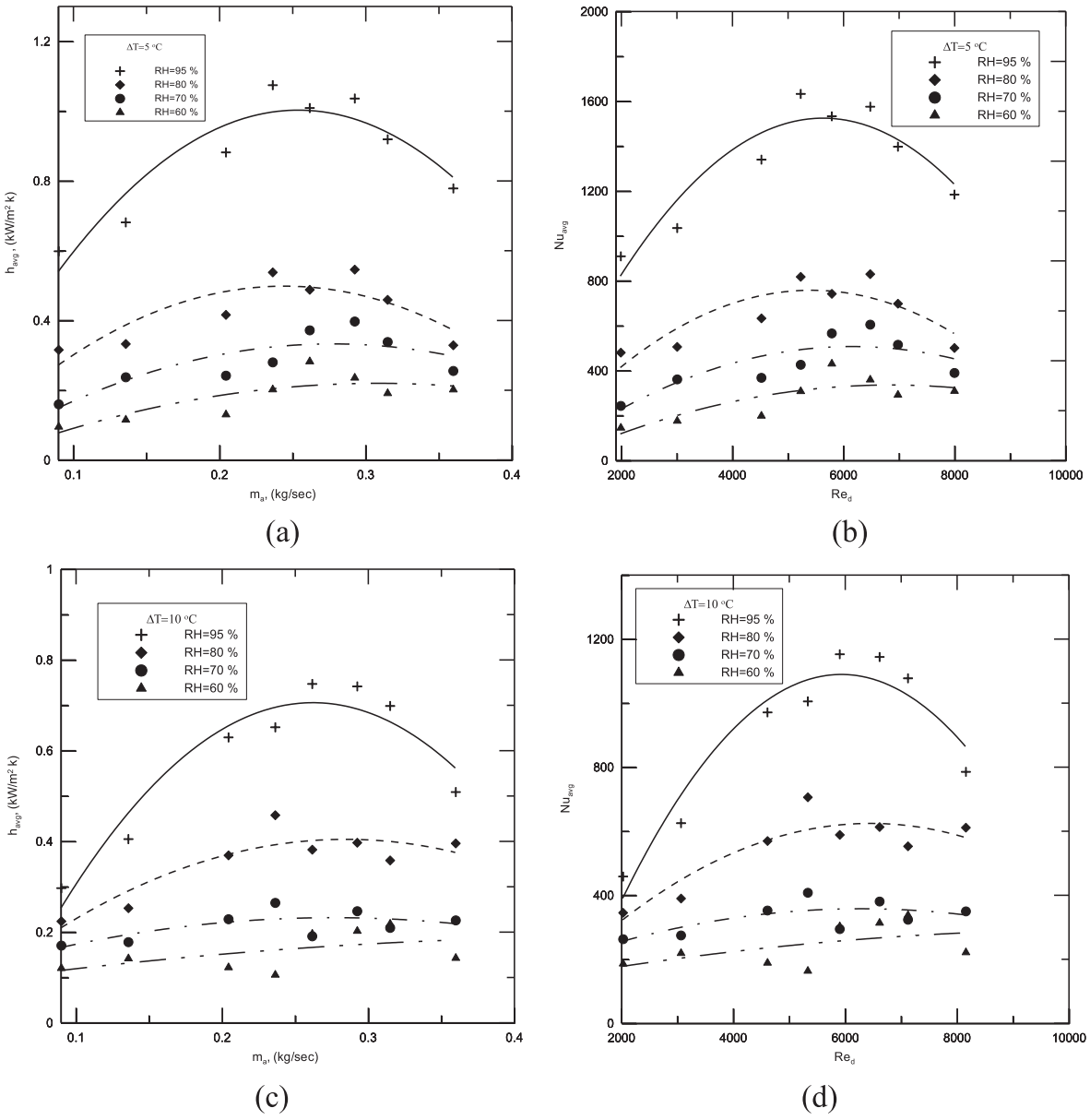

Fig. 15. Heat transfer coefficient of moist air for different values of air relative humidity at: (a) & (b) $\Delta T = 5$ °C, (c) & (d) $\Delta T = 10$ °C.

studied parameter is plotted in Fig. 14a and b at ΔT equals 5 °C & 10 °C, respectively. As shown in the figures at any RH and $\dot{m}_a < 0.29$ kg/s, the condensation rate enhanced with increasing the air mass flow rate, otherwise, it reduces with increasing $\dot{m}_a$. Increasing the air mass flow rate up to 0.29 kg/s improves both heat and mass transfer coefficients and consequently the rate of condensate increases. But, with further mass flow rate $\dot{m}_a > 0.29$, the condensation rate decreases due to higher air velocity which causes an entrainment to part of condensate downstream the test section. Moreover, the condensate changes from drop wise to film wise state, hence, the heat and mass transfer decreases. In addition to, the condensation rate improves with increasing air relative humidly and ΔT as can be seen in Fig. 14a and b. Moreover the rate of condensation increases significantly for RH > 80%.

4.2.2. Heat and mass transfer coefficients

The heat and mass transfer coefficients and corresponding average Nusselt and Sherwood numbers versus the air mass flow rate at different air inlet relative humidity ranges from 60% to 95% as a studied parameter is plotted at different ΔT (5 °C & 10 °C) as presented in Figs. 15 and 16. It can be observed that the RH and ΔT have remarkable effect on heat and mass transfer coefficients and corresponding Nu_{avg} and Sh_{avg}, where the heat transfer and mass transfer coefficients improve with higher RH and lower ΔT. Increasing RH enhances the rate of condensation, hence the heat and mass transfer coefficients improve, in other side the drop wise condensate accompanied with smaller ΔT and the higher heat and mass transfer coefficients can be obtained. Furthermore, the effects of air mass flow rates on h_{avg} & $h_{m,avg}$ and corresponding Nu_{avg} and

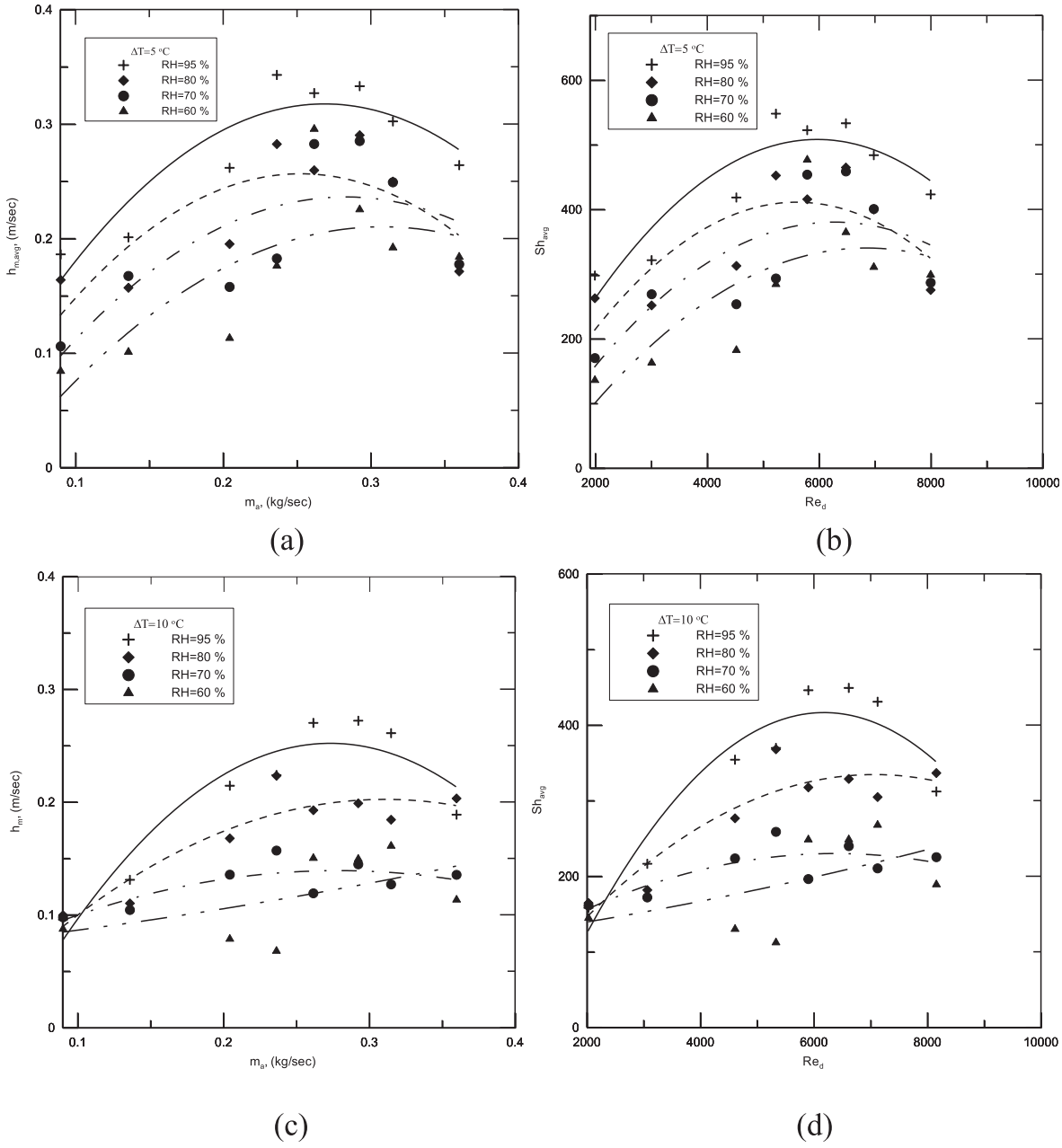

Fig. 16. Mass transfer coefficient of moist air for different values of air relative humidity at: (a) & (b) $\Delta T = 5$ °C, (c) & (d) $\Delta T = 10$ °C.

Sh_{avg} are the same as on the rate of condensation and the trends are similar.

4.3. Comparisons

Fig. 17a and b show comparisons between present theoretical and experimental results for average Nusselt and Sherwood numbers, respectively. As shown in the figures, the experimental Nu_{avg} and Sh_{avg} are higher than theoretical values; this can be attributed to inherent assumptions in theoretical model. In the theoretical model, the pipe surface temperature is constant and equals air dew point, but in the experimental work the pipe surface temperature is varied and lower than air dew point. In addition to, the condensate in experimental work is drop wise state on the pipe outer surface that means an increase in the heat transfer surface area and consequently an increase in the heat and mass transfer coefficients. While, in theoretical modeling the condensation is considered as a liquid film wise on the pipe outer surface. Further comparisons are presented in Fig. 18a and b, a comparison between present and previous theoretical results [3] is illustrated in Fig. 18a, while a comparison between present experimental results and previous theoretical results [3] is seen in Fig. 18b. As shown in the figures the present theoretical and experimental works give

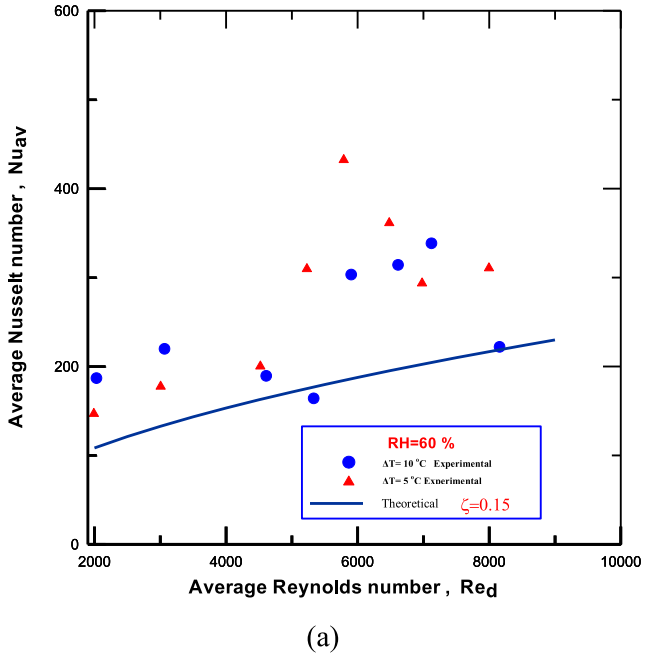

Fig. 17. Comparison between present theoretical and experimental results for (a) Nu_{avg}, (b) Sh_{avg}.

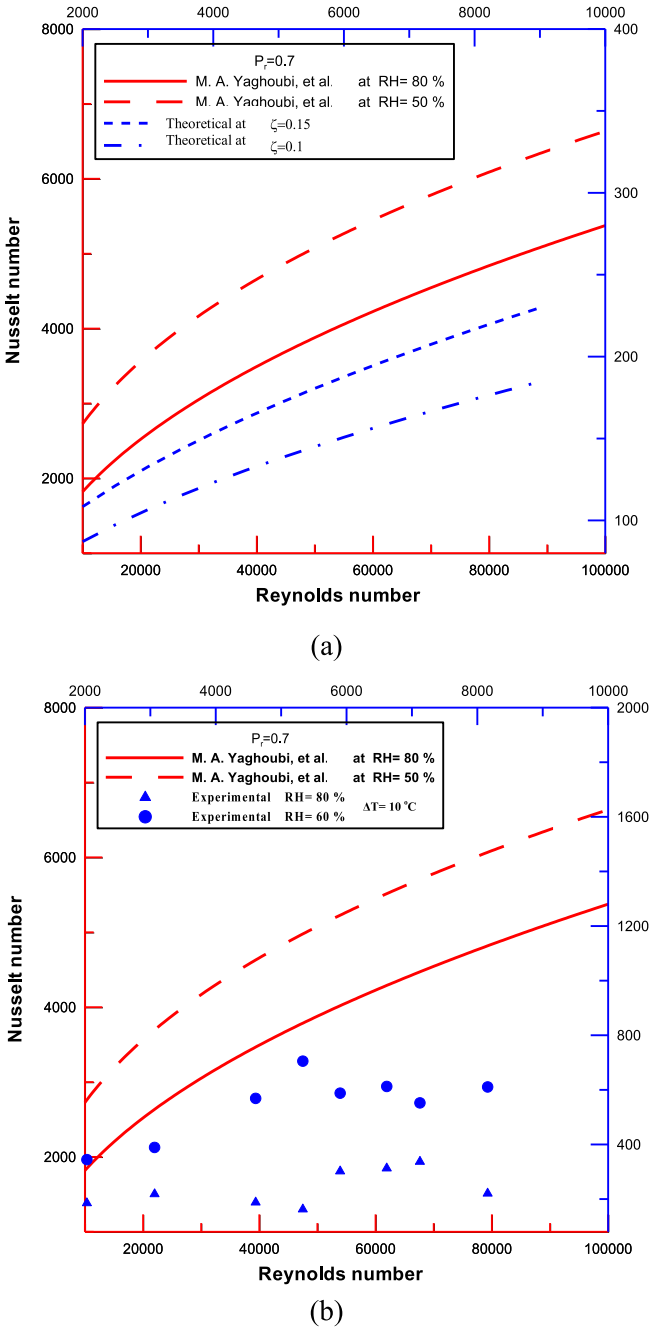

Fig. 18. Comparisons between: (a) present theoretical with previous theoretical results, (b) present experimental with previous theoretical results.[3].

satisfactory agreement trends with the previous theoretical study, in spite of it gives higher values than the present work. The discrepancies are due to that the previous theoretical work was carried out on condensation process over flat plate surface with higher ranges of Reynolds number.

4.4. Numerical and experimental correlations

Nusselt and Sherwood numbers correlations can be correlated numerically from numerical solution of ODEs from Eq. (15)–(17) as illustrated in Fig. 19a and b in terms of *Pr*, *Re*, ζ, for Nu_x and *Sc*, *Re* for Sh_x as follows:

$$Nu_x = 4.72 Pr^{0.33}\ Re_x^{0.5}\ \zeta^{0.51} \tag{35}$$

The Eq. (35) can predict 85% of the numerical results within error ±6% for the following ranges: $Pr = 0.7$, $\xi = 0.05$, $0.0 < Re_x \le 9000$, and $0.005 \le \zeta \le 0.15$

$$Sh_x = 0.635\ Sc^{0.33}\ Re_x^{0.5} \xi^{0.089} \tag{36}$$

The Eq. (36) can predict 100% of the numerical results with negligible error for the following ranges: $Sc = 0.7$, $0.0 < Re_x \le 9000$, and $0.005 \le \xi \le 0.15$

Similarly, the experimental data are regressed to obtain Nu_{avg} and Sh_{avg} as illustrated in Fig. 20a and b in terms of *Pr*, Re_d, RH_{in}, and TR for Nu_{avg} and *Sc*, Re_d, RH_{in}, and TR for Sh_{avg} within ranges of 60% $\le RH_{in} \le$ 95%, 2000 $\le Re_d \le$ 8000, 5°C $\le \Delta T \le$ 10°C, and $Pr = Sc =$ 0.7 are given as follows:

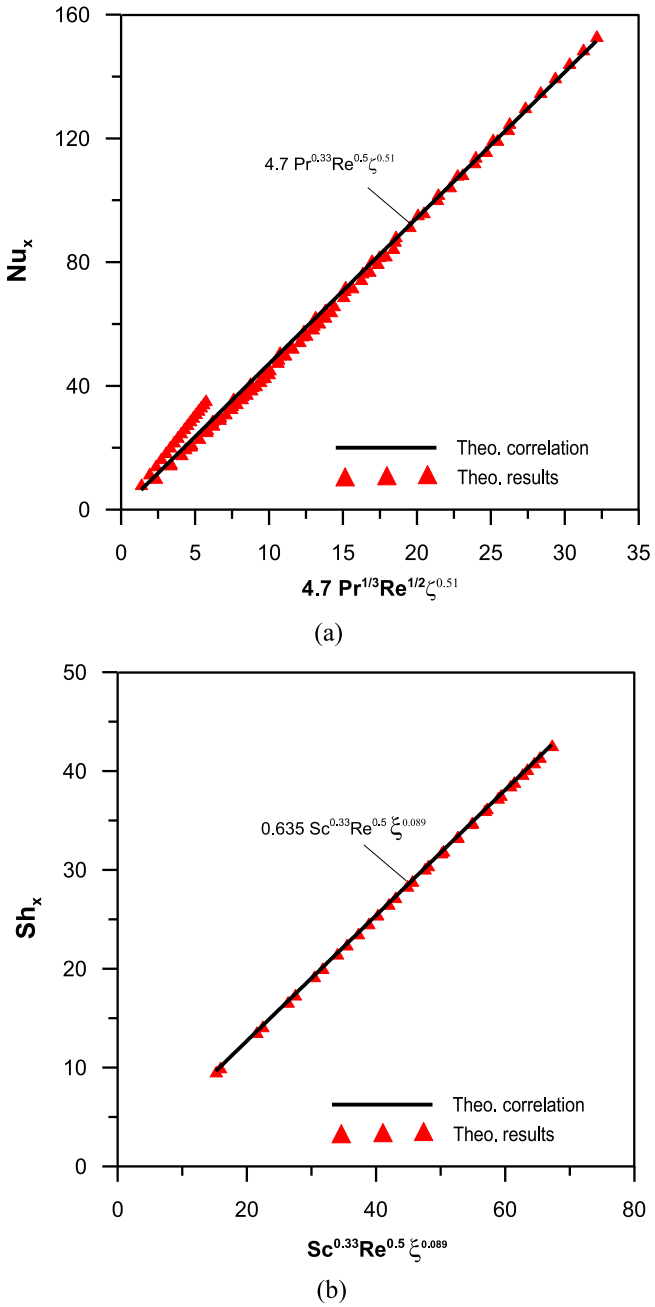

Fig. 19. Theoretical correlations prediction for (a) Nusselt number, (b) Sherwood number.

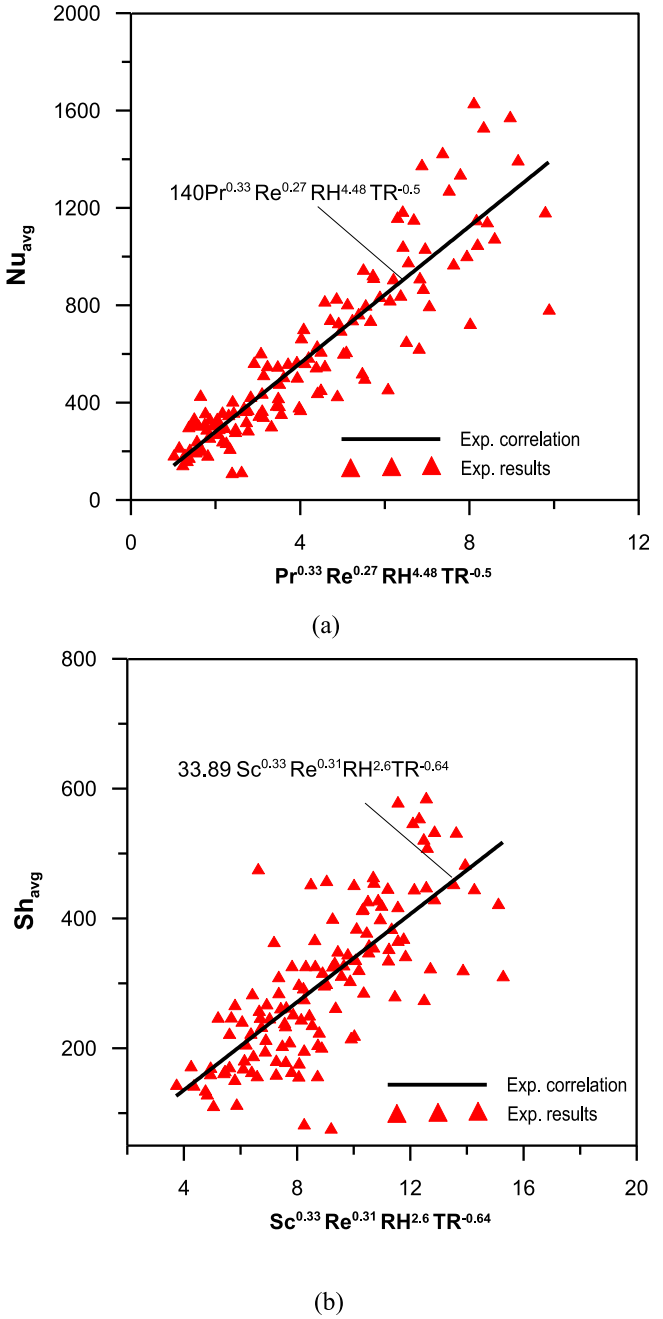

Fig. 20. Experimental correlations prediction for (a) Nusselt number, (b) Sherwood number.

$$Nu_{avg} = 140.5 Pr^{0.33} Re_d^{0.27} RH_{in}^{4.48} TR^{-0.5} \quad (37)$$

The Eq. (37) can predict 75% of the experimental data within error ±25%:

$$Sh_{avg} = 33.89 Sc^{0.33} Re_d^{0.31} Re_{in}^{2.6} TR^{-0.64} \quad (38)$$

The Eq. (38) can predict 72% of the experimental data within error ±25%

5. Conclusions

Theoretical and experimental study for investigating the condensation process of moist air around horizontal pipe have been carried out to present the effects of air inlet conditions on the heat and mass transfer coefficients. The conclusions obtained from the present study are listed briefly as follows:

- The separation point occurs at higher position angle with increasing Reynolds number, where, the separation point approximately equals 170° for studied parameters.
- The condensation parameter, ζ has a considerable effect on thermal boundary layer thickness, η_t, but the position parameter, ξ has a negligible effect on it.
- Both of Prandtl Numbers, Pr and condensation parameter, ζ have remarkable effects on the local Nusselt number, Nu_x, whereas, Local Sherwood number, Sh_x is significantly influenced by Schmidt number, Sc and position parameter, ξ.
- The condensation rate improves with increasing air mass flow rate, air relative humidly, and ΔT. Whereas, it reduces with increasing air mass flow rate for $\dot{m}_a > 0.29$ kg/s
- The heat and mass transfer coefficients, h_{avg} & $h_{m,avg}$ and corresponding Nu_{avg} & Sh_{avg} improved with higher RH and lower ΔT.
- Comparisons between the present theoretical and experimental works and with previous theoretical study were conducted and they gave satisfactory agreement trends.
- Theoretical and experimental correlations for Nusselt and Sherwood numbers are developed and presented in terms of studied parameters.

References

[1] E.S. Gaddis, Solution of the two phase boundary layer equations for laminar film condensation of vapour flowing perpendicular to a horizontal cylinder, Int. J. Heat Mass Transfer 22 (1979) 371–382.
[2] J.W. Rose, Effect of pressure gradient in forced convection film condensation on horizontal tube, Int. J. Heat Mass Transfer 27 (1984) 39–47.
[3] M.A. Yaghoubi, H. Kazeminejad, A. Farshidiyanfar, Heat and mass transfer with dehumidification in laminar boundary layer flow along a cooled flat plate, Int. J. Heat Transfer 115 (1993) 785–790.
[4] F. Legay-Desesquelles, B. Prunet-Foch, Dynamic behaviour of a boundary layer with condensation along a flat plate: comparison with suction, Int. J. Heat Mass Transfer 28 (1985) 2363–2370.
[5] Pedro J. Mago, S.A. Sherif, Heat and mass transfer on a cylinder surface in cross flow under supersaturated frosting conditions, Int. J. Refrig. 26 (2003) 889–899.
[6] T.S. Chen, C.F. Yuh, Combined heat and mass transfer in mixed convection along vertical and inclined flat plates, Int. J. Heat Mass Transfer 23 (1980) 527–537.
[7] L.C. Chow, J.N. Chung, Evaporation of water into a laminar stream of air and superheated steam, Int. J. Heat Mass Transfer 26 (1983) 373–380.
[8] U.K. Ghosh, S.N. Gupta, S. Kumar, S.N. Upadhyay, Mass transfer in cross flow of non Newtonian fluid around a circular cylinder, Int. J. Heat Mass Transfer 29 (1986) 955–960.
[9] F. Legay-Desesquelles, B. Prunet-Foch, Heat and mass transfer with condensation in laminar and turbulent boundary layer along at flat plat, Int. J. Heat Mass Transfer 29 (1986) 95–105.
[10] Wel-Mon Yan, Transport phenomena of developing laminar mixed convection heat and mass transfer in inclined rectangular ducts, Int. J. Heat Mass Transfer 38 (1995) 2905–2914.
[11] F. Mendez, C. Trevino, Film condensation induced by a natural convective flow: steady analysis, Int. J. Heat Mass Transfer 40 (1997) 1279–1289.
[12] Kuan-Tzong Lee, Wei-Mon Yan, Mixed convection heat transfer in horizontal rectangular ducts with wall transpiration effects, Int. J. Heat Mass Transfer 41 (1998) 411–423.
[13] F. Mendez, J.J. Lizardi, C. Trevino, Laminar film condensation along a vertical fin, Int. J. Heat Mass Transfer 43 (2000) 2859–2868.
[14] Kikuji Chida, Surface temperature of a flat plate of finite thickness under conjugate laminar forced convection heat transfer condition, Int. J. Heat Mass Transfer 43 (2000) 639–642.
[15] Man-Hoe Kim, Sumin Song, Clark W. Bullard, Effect of inlet humidity condition on the air-side performance of an inclined brazed aluminum evaporator, Int. J. Refrig. 25 (2002) 611–620.
[16] N. Mendes, F.C. Winkelmann, R. Lamberts, P.C. Philippi, Moisture effects on conduction loads, Int. J. Energy Build. 35 (2003) 631–644.
[17] W.R. Foss, C.A. Bronkhorst, K.A. Bennett, Simultaneous heat and mass transport in paper sheets during moisture sorption from humid air, Int. J. Heat Mass Transfer 46 (2003) 2875–2886.
[18] M.M. Hussain, I. Dincer, Two-dimensional heat and moisture transfer analysis of a cylinder moist object subjected to drying: a finite-difference approach, Int. J. Heat Mass Transfer 46 (2003) 4033–4039.
[19] E.P. Volchkov, V.V. Terekhov, V.I. Terekhov, A numerical study of boundary-layer heat and mass transfer in a forced flow of humid air with surface steam condensation, Int. J. Heat Mass Transfer 47 (2004) 1473–1481.
[20] Zouhair Ait Hammou, Brahim Benhamou, Nicolas Galanis, Jamel orfi, laminar mixed convection of humid air in a vertical channel with evaporation or condensation at the wall, Int. J. Therm. Sci. 43 (2004) 531–539.
[21] Worachest Pirompugd, Somchai Wongwises, Chi-Chuan Wang, Simultaneous heat and mass transfer characteristics for wavy fin and tube heat exchangers under dehumidifying conditions, Int. J. Heat Mass Transfer 49 (2006) 132–143.
[22] Shripad T. Revankar, Doug Pollock, Laminar film condensation in a vertical tube in the presence of noncondensable gas, Appl. Math. Model. 29 (2005) 341–359.
[23] L.I. Cheng, L.I. Junming, Laminar forced convection heat and mass Transfer of humid air across a vertical plate with condensation, Chin. J. Chem. Eng. 19 (6) (2011) 944–954.
[24] Wilson Terrell Jr., Ty A. Newell, Experimental techniques for determining heat and mass transfer due to condensation of humid air in cooled, open cavities, Appl. Therm. Eng. 27 (2007) 1574–1584.
[25] Kei Sakakura, Satoru Yamamoto, Numerical and experimental predictions of heterogeneous condensate flow of moist air in cooled pipe, Int. J. Heat Fluid Flow 27 (2006) 220–228.
[26] Xiaojun Ma, Xianting Li, Xiaoliang Shao, Xuan Jiang, An algorithm to predict the transient moisture distribution for wall condensation under a steady flow field, Build. Environ. 67 (2013) 56–68.
[27] Zhixiang Zhao, Yanzhong Li, Lei Wang, Zhan Liu, Jiang Zheng, Flow and heat transfer characteristics of ambient air condensation on a horizontal cryogenic tube, Cryogenics 62 (2014) 110–117.
[28] Q.T. Le, S.J. Ormiston, H.M. Soliman, A closed-form solution for laminar film condensation from quiescent pure vapours on curved vertical walls, Int. J. Heat Mass Transfer 73 (2014) 834–838.
[29] J.P. Holman, W.J. Gajda, Experimental Method for Engineers, McGraw Hill, New York, 1994.
[30] Koh, Laminar film condensation of condensable gases and mixtures on a flat plate, Proc. 4th U. S. A. Nat. Congr. Appl. Mech. 2 (1961) 1327–1336.
[31] Sparrow, et al., Forced convection condensation in the presence of non-condensables and interface resistance, Int. J. Heat Mass Transfer 10 (1967) 1829–1845.
[32] Berman, Determination of mass transfer coefficient in calculations on steam containing air, Teploenergetica 16 (1969) 68–71.
[33] Mills, et al., Experimental study of steam-air mixtures flowing over a horizontal tube, Proc. 5th Int. Heat Transfer Conf. 5 (1974) 20–23.
[34] Rose, Approximate equations for forced convection condensation in the presence of a non-condensing gas on a flat plate and horizontal tube, Int. J. Heat Mass Transfer 23 (1980) 539–546.